

Three-dimensional Relativistic MHD Simulations of Active Galactic Nuclei Jets: Magnetic Kink Instability and Fanaroff-Riley Dichotomy

Alexander Tchekhovskoy^{1,2*} † and Omer Bromberg^{3‡}

¹*Departments of Astronomy and Physics, Theoretical Astrophysics Center, University of California Berkeley, Berkeley, CA 94720-3411*

²*Lawrence Berkeley National Laboratory, 1 Cyclotron Rd, Berkeley, CA 94720, USA*

³*Department of Astrophysical Sciences, Peyton Hall, Princeton University, Princeton, NJ 08544, USA*

Accepted. Received; in original form

ABSTRACT

Energy deposition by active galactic nuclei jets into the ambient medium can affect galaxy formation and evolution, the cooling of gas flows at the centres of galaxy clusters, and the growth of the supermassive black holes. However, the processes that couple jet power to the ambient medium and determine jet morphology are poorly understood. For instance, there is no agreement on the cause of the well-known Fanaroff-Riley (FR) morphological dichotomy of jets, with FRI jets being shorter and less stable than FR II jets. We carry out global 3D magnetohydrodynamic simulations of relativistic jets propagating through the ambient medium. We show that the flat density profiles of galactic cores slow down and collimate the jets, making them susceptible to the 3D magnetic kink instability. We obtain a critical power, which depends on the galaxy core mass and radius, below which jets become kink-unstable within the core, stall, and inflate cavities filled with relativistically-hot plasma. Jets above the critical power stably escape the core and form powerful backflows. Thus, the kink instability controls the jet morphology and can lead to the FR dichotomy. The model-predicted dependence of the critical power on the galaxy optical luminosity agrees well with observations.

Key words: galaxies: active — galaxies: jets — magnetic fields — instabilities — MHD

1 INTRODUCTION

Active galactic nuclei (AGN) jet interaction with the interstellar/intergalactic medium (ISM/IGM) is very rich and exhibits different types of morphology of poorly understood origin. Some jets appear conical, show large-scale wiggles, decelerate due to the interaction with the ambient medium (Laing 1993; Laing & Bridle 2002), like the M87 jet (Hines, Eilek, & Owen 1989). Their extended emission at 1.4 GHz tends to peak less than half-way from the nucleus to the outer edge; such jets are classified as FRI jets (Fanaroff & Riley 1974). FR II jets appear nearly straight, edge brightened, and end up in a hot spot, like the Cygnus A jet (Perley et al. 1984). They are generally more powerful than FRI jets (Owen & Ledlow 1994; Ledlow & Owen 1996, with recent revisions, Best 2009) and preferentially occur in isolated, field galaxies (see Hagino et al. 2015, and references therein). Although on average FR II jets are more spatially extended than FRI jets, some FRI jets reach Mpc distances (Hardcastle et al. 2002; Laing et al. 2008).

There is no agreement on the physical reasons leading to the FRI/FR II dichotomy. These could include differences in the central engine (e.g., Baum, Zirbel, & O’Dea 1995; Meier 1999) and ambi-

ent medium (e.g., Gopal-Krishna & Wiita 2000). Whereas the FR II morphology was reproduced by pioneering hydrodynamic simulations (Clarke, Norman, & Burns 1986), the apparent instabilities of FRI jets and their observed deceleration are much more difficult to explain. Some of the possibilities include Kelvin-Helmholtz (KH) instabilities in the shear layers (e.g., Kaiser & Alexander 1997, hereafter KA97; Perucho, Martí, & Hanasz 2005; Meliani & Kepens 2009; Perucho et al. 2010), and mass entrainment from stellar winds (Komissarov 1994; Perucho et al. 2014; Wykes et al. 2015).

Magnetic fields are natural candidates to launch relativistic jets (e.g. Tchekhovskoy, Narayan, & McKinney 2011). Inferred to be dynamically-important in the central regions of many radio-loud AGN (Zamaninasab et al. 2014; Ghisellini et al. 2014; Nemmen & Tchekhovskoy 2015), they may affect jet morphology by suppressing KH mixing and initiating current-driven instabilities, e.g., the 3D magnetic kink (“corkscrew”) instability (Nakamura, Li, & Li 2007; Mignone et al. 2010; Mizuno et al. 2012; Guan, Li, & Li 2014; Porth & Komissarov 2015, hereafter PK15; Bromberg & Tchekhovskoy 2016, hereafter BT16). This motivates a detailed 3D study of magnetic effects on the global dynamics of jet-ISM/IGM interaction. Extra care needs to be taken in the way magnetic jets are initiated. In particular, different values of the magnetic pitch, or the ratio of poloidal to toroidal magnetic field, B_p/B_ϕ , at the injection point result in different jet morphologies (Guan et al. 2014). To eliminate this uncertainty, we follow BT16 and set up our simula-

* E-mail: atchekho@berkeley.edu, omerb@astro.princeton.edu

† Einstein Fellow

‡ Lyman Spitzer, Jr. Fellow

Table 1. Simulation setup parameters for the various models we present.

Model name	Resolution ($N_r \times N_\theta \times N_\phi$)	ν	Λ_{in}	r_{in}	r_{out}	r_{break}	$\frac{ct_{\text{sim}}}{r_{\text{in}}}$
P46	$256 \times 96 \times 192$	1	9.3	1	10^8	–	2.1×10^4
P46B2	$256 \times 96 \times 192$	1	9.3	1	10^5	10^2	2.1×10^4
P44	$256 \times 96 \times 192$	1	4.3	1	10^5	–	5.4×10^4
P44HR	$320 \times 96 \times 192$	1.4	4.3	1	10^3	–	3.4×10^4

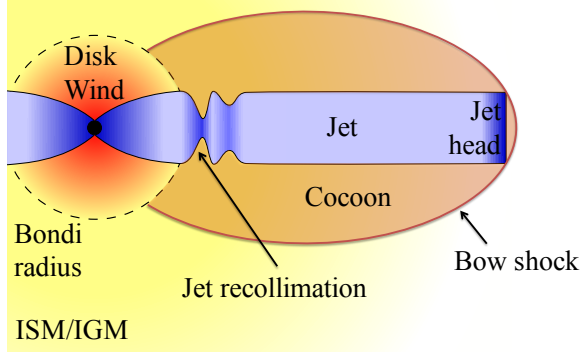


Figure 1. Cartoon depiction of an AGN central engine. The jets (blue) collimate against the accretion disc wind (red) and assume a parabolic shape inside the Bondi radius (dashed line). Once outside, they start interacting with the ambient medium (ISM/IGM, shown in yellow). As the jets adjust to this change in the ambient density profile, they go through a series of recollimation events and eventually settle into a near-cylindrical configuration. At its head, the jet drills through the ISM/IGM and sends out a bow shock. The shocked ambient medium and the jet exhaust form a cocoon (brown) that collimates the jet outside the Bondi radius.

tions to launch the jets the way nature does it: via the magnetised rotation of a central object. We give numerical details in Section 2, present our results in Section 3, and conclude in Section 4.

2 NUMERICAL METHOD AND PROBLEM SETUP

We use global time-dependent relativistic 3D magnetohydrodynamic (MHD) numerical simulations in order to study the propagation of magnetised jets in an ambient medium characteristic of AGN. We carry out the simulations with the `HARM` code (Gammie, McKinney, & Tóth 2003; Noble et al. 2006; Tchekhovskoy et al. 2007; McKinney & Blandford 2009; Tchekhovskoy et al. 2011 and use modified spherical polar coordinates (r, θ, φ) described below that span the range $(r_{\text{in}}, r_{\text{out}}) \times (0, \pi) \times (0, 2\pi)$.

Fig. 1 shows a cartoon of the AGN. Within the *Bondi radius*, $r < r_B$, the thermal pressure of the ISM/IGM cannot support the gas against gravity. Here, black hole (BH) powered jets propagate unimpeded, are collimated by the accretion disc wind, and have a parabola-like shape, as seen in the M87 galaxy (Nakamura & Asada 2013) and the numerical simulations of jet formation (McKinney 2006; Hawley & Krolik 2006; Tchekhovskoy, Narayan, & McKinney 2011; Tchekhovskoy, McKinney, & Narayan 2012; Tchekhovskoy & McKinney 2012; Tchekhovskoy 2015). At $r \gtrsim r_B$, the jet shape is observed to change from parabolic to conical, at least for the M87 galaxy (Nakamura & Asada 2013). It is plausible that around this distance the jets start to interact with the ISM/IGM, causing them to undergo a series of recollimations (BT16) that appear as a series of stationary features, such as HST-1, seen in the M87 jet (Biretta, Sparks, & Macchetto 1999; Meyer et al. 2013).

Table 2. Simulations scaled to physical systems of different size and power. We indicate scaled versions of the models with suffixes.

Model name	Suffix	Λ_{in}	r_{in} [kpc]	r_{out} [kpc]	r_{break} [kpc]	n_{kpc} [cm^{-3}]	$L_j / 10^{45}$	t_{sim} [Myr]
P46		9.3	0.1	10^4	–	0.2	15	6.7
P46B2		9.3	0.1	10^4	10	0.2	15	6.7
P44		4.3	0.1	10^4	–	0.2	0.15	17
P44	nx5	4.3	0.1	10^4	–	1.0	0.75	17
P44	rx5	4.3	0.5	5×10^4	–	0.2	0.75	85

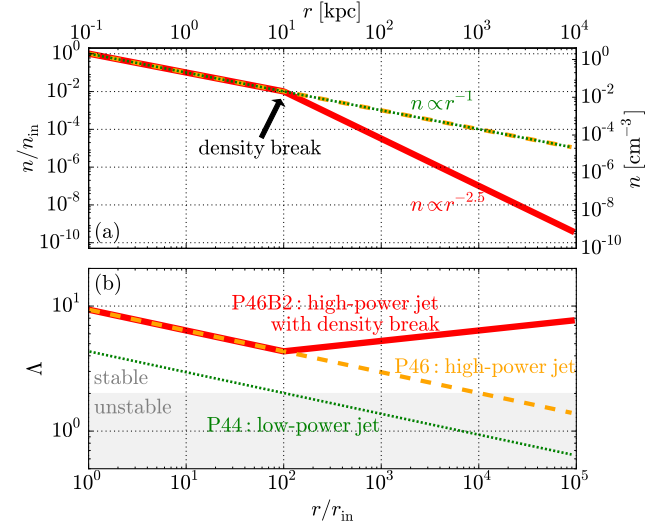


Figure 2. (panel a): Ambient medium density profiles of our simulations. We consider flat power-law density profiles at small distances ($n \propto r^{-1}$) that, in some models, steepen at larger radii ($n \propto r^{-2.5}$) to mimic the edge of the galaxy/cluster core. (panel b): Jet stability parameter versus radius in our simulations. The high-power jets maintain stability out to Mpc distances, whereas the low-power jets are expected to become unstable around 10 kpc.

Motivated by this, our fiducial choice for the position of the inner radial boundary r_{in} is the Bondi radius, which we take to be $r_B = 0.1$ kpc (see, e.g., Russell et al. 2015), and place the outer boundary at a large distance, $r_{\text{out}} \gg r_{\text{in}}$, so that the transients do not reach it in a simulation time (see Tab. 1). We fill the domain with a cold, spherically-symmetric density distribution described in Sec. 3 and neglect gravity. We model the inner boundary as a perfectly conducting magnetised sphere threaded with a laterally-uniform radial magnetic flux.¹ At the beginning of the simulation, we spin the polar caps of the sphere within 50° of the rotational axis at an angular frequency $\Omega = 0.8c/r_{\text{in}}$. The initiation of jets via the rotation at the base leads to a natural degree of magnetic field azimuthal winding, a crucial factor that controls the stability of magnetised jets (BT16). The jets are initially highly magnetised, with magnetisation at the inner radial boundary, $\sigma \equiv 2p_m/\rho c^2 = 25 \gg 1$, where p_m is the magnetic pressure and ρ is the fluid-frame mass density in the jet.

¹ To avoid the interaction of the jets with the polar singularity, we orient the rotational axis along the x -direction and collimate the radial grid lines toward it in order to resolve the jets well, with the angle that a radial grid line makes with the x -axis scaling as $\chi \propto r^{-\nu/2}$ (see BT16, for details).

3 KINK MODE AND JET MORPHOLOGY

Of current-driven, 3D instabilities, the most serious is the kink ($m = 1$) mode. It causes the jets to move bodily sideways and develop helical motions (Appl, Lery, & Baty 2000; Narayan, Li, & Tchekhovskoy 2009). To evaluate its potential to disrupt the jets, BT16 computed the ratio of the instability growth timescale, evaluated as the time it takes an Alfvén wave to travel around the jet 10 times, to the time for a fluid element to travel from the base to the tip of the jet. This gives us the stability parameter,

$$\Lambda = 2 \frac{\gamma_j \theta_j}{0.03} = K \times \left(\frac{L_j}{n m_p r^2 \gamma_j^2 c^3} \right)^{1/6}, \quad (1)$$

where, n is the ambient medium number density, m_p is the proton mass, r is the distance along the jet, $K = 20(2\pi/9)^{1/2}[\pi(5 - \alpha)(3 - \alpha)/6]^{1/3}$ is a constant prefactor, and $\alpha = -d \log n/d \log r$ is the slope of the ambient density profile (BT16). Unless stated otherwise, we will assume that the jet plasma moves at a mildly relativistic velocity, $\beta_j \equiv v_j/c \approx 1$ and $\gamma_j \equiv (1 - \beta_j^2)^{-1/2} \approx 1$, and is highly magnetised, $\sigma \gg 1$. Equation (1) shows that tightly collimated jets are the most susceptible to the kink instability: in fact, if $\Lambda \lesssim \Lambda_{\text{crit}} \equiv 2$, or $\theta_j \lesssim \theta_{\text{crit}} \equiv 0.03/\gamma_j$, the kink instability has sufficient time to develop and can disrupt the jets and cause them to stall (BT16).

We consider two fiducial models: model P44, representative of a weak FRI-like jet of power $L_j \approx 1.5 \times 10^{44}$ erg s $^{-1}$, and model P46, representative of a powerful FR II-like jet of $L_j \approx 1.5 \times 10^{46}$ erg s $^{-1}$. Figure 2(a) shows the chosen initial ambient density profile: a power-law, $n = n_{\text{kpc}}(r/\text{kpc})^{-\alpha}$, with normalisation $n_{\text{kpc}} = 0.2 \text{ cm}^{-3}$ and slope $\alpha = 1$ characteristic of cores of elliptical galaxies such as M87 (see Tab. 1 and Stewart et al. 1984; Russell et al. 2015). Since the jets in powerful FR II sources often leave the host galaxy/cluster core, we consider model P46B2 with a steeper density profile outside of the core, $r > r_{\text{break}}$, where the density is multiplied by a factor $(r/r_{\text{break}})^{-1.5}$. We adopt $r_{\text{break}} = 10^2 r_{\text{in}}$, leading to a sufficient scale separation between r_{in} and r_{break} (see Fig. 2 and Tab. 1). By changing the length unit while holding $\Lambda_{\text{in}} = \Lambda(r_{\text{in}})$ constant, our simulations can be rescaled to different jet powers and ambient densities (see models P44nx5 and P44rx5 in Tab. 2).

As the jets run into the ISM/IGM, their dynamics is regulated by their ability to drill through the ambient gas. In flat density profiles with $\alpha < 2$, the mass per unit distance ahead of the jets increases with distance. This causes the jets to slow down and collimate into smaller opening angles, and become less stable, $\theta_j \propto \Lambda \propto r^{-(2-\alpha)/6}$ (see eq. 1 and Fig. 2b). Hence, in an $\alpha = 1$ environment, such as in models P44 and P46, jets eventually become unstable, reaching $\theta_j \lesssim \theta_{\text{crit}}$ or equivalently $\Lambda \lesssim 2$ (shaded area in Fig. 2b). This occurs at a critical distance (BT16),

$$r_{\text{crit}} = 7 \text{ kpc} \times \left(\frac{L_j}{10^{44} \text{ erg s}^{-1}} \times \frac{0.2 \text{ cm}^{-3}}{n_{\text{kpc}}} \right)^{1/(2-\alpha)}. \quad (2)$$

Fig. 2(b) shows that in the low-power model P44 the jets cross into the unstable region at $r \gtrsim 10$ kpc. In contrast, in the high-power model P46 the jets maintain $\Lambda > 2$ until Mpc-scales, suggesting that they remain stable out to these large distances. In the model with the density break, P46B2, the jets never cross into the instability region: as they enter the steep density profile region ($\alpha > 2$), they become progressively more stable as they propagate away. To sum up, we expect low-power jets to become unstable and disrupt well within the galaxy/cluster cores, and the high-power jets to remain stable out to large distances, well outside the galaxy.

Fig. 3 quantifies jet stability to current-driven 3D instabilities by showing the position of jet head versus time for the first three

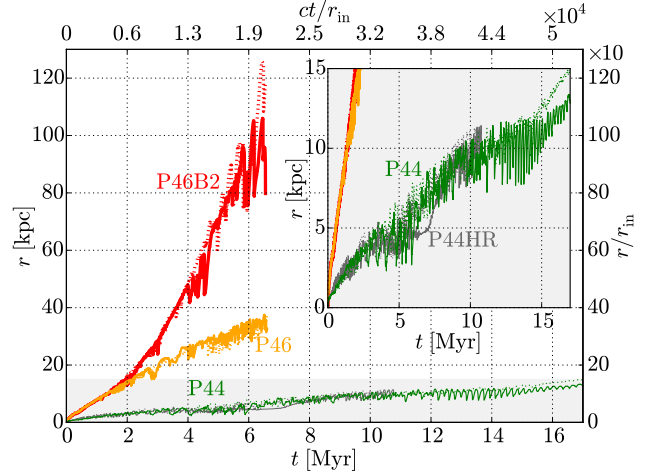


Figure 3. Position of jet head versus time in different models considered in this work. Solid lines show the right and dotted lines left jet. The high-power jet with the density break (model P46B2, red lines), reaches ~ 100 kpc and that without the density break (model P46, orange lines), reaches ~ 30 kpc after 6 Myr. The inset shows with the green lines the zoom-in on the low-power jet model, P44, in which the jet propagates approximately 10 times slower and stalls at $t \sim 3\text{--}6$ Myr, with the head position showing large-amplitude oscillations around $r \sim 5$ kpc. As a result, the jet inflates large cavities seen in Fig. 4(c). Shown in grey, jet head position in the model P44HR, which has twice as high effective resolution in all 3 dimensions, closely tracks that in the model P44; hence our models are well-resolved.

models in Tables 1 and 2. The jets in the high-power model P46 decelerate, as expected in flat density profiles with $\alpha < 2$ (BT16). Similarly, the jets in model P46B2 decelerate within the flat density core, $r < r_{\text{break}} = 10$ kpc, but accelerate outside, as the density slope steepens to $\alpha = 2.5$. As a result, at 6 Myr the jets in model P46B2 reach $r \sim 100$ kpc, three times larger than in model P46.

Figs 4(a) and 4(b) show that the powerful jets in models P46B2 and P46, respectively, retain their overall stability and display the morphology characteristic of powerful FR II sources: mostly straight, well-defined jets all the way to the points at which they drill through the ambient medium (“hot spots”) and form powerful backflows. Thus, so long as the jets are powerful enough, the details of the ambient density profile do not have a very strong effect on the jet morphology. Note that the global kink instability causes the jets to exhibit large-scale bends similar to those seen in some FR II sources such as Cygnus A (Perley et al. 1984). Our simulations show that such bends naturally develop as a result of global magnetic instabilities caused by the interaction of the jets with the ambient medium, even without any asymmetries imposed on the jets as they emerge from the central engine.

The jets in the low-power model P44 show a qualitatively different behaviour. The inset in Fig. 3 shows a zoom-in on the jet head dynamics in the model P44. At early times, the jets propagate in a similar way to high-power jets: their velocity decreases as they propagate away from the centre. However, in qualitative agreement with the estimate (2), once the jets approach a critical distance, $r_{\text{crit}} \sim 5$ kpc, a violent kink instability sets in and stalls their propagation for a time comparable to the jet lifetime. The inset in Fig. 3 shows that the stall occurs over the time range $t = 3\text{--}6$ Myr that is comparable to the interval, inferred to be ~ 10 Myr, between the subsequent outbursts in M87 (Million et al. 2010). Thus, at present M87 jets are likely to be stalled by the kink instability.

Fig. 4(c) shows that the stalled low-power jets in model P44

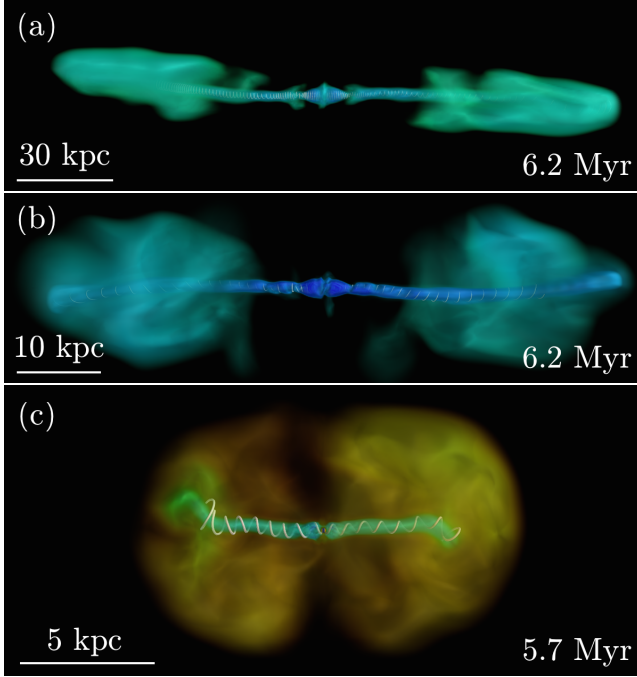


Figure 4. Volume rendering of simulated jets shows the logarithm of density (yellow-green shows high and blue shows low values). White lines show magnetic field lines. Please see Supporting Information and YouTube (link) for the movies. (panel a): High-power jets in model P46B2 reach 100 kpc distances in 6 Myr. They are mostly straight apart from subtle, large-scale bends seen in FRII sources such as Cygnus A; after running into the ambient medium, the jets end up forming strong backflows, as characteristic of FRII jet sources. (panel b): High-power jets in model P46 reach 30 kpc in 6 Myr. Their backflows are less well-collimated than in model P46B2. (panel c): Low-power jets in model P44, reach a distance of 5 kpc in 3 Myr. Once there, they succumb to a global kink instability and remain stalled at this distance for 3 Myr (see Fig. 3). These jets inflate large cavities (shown in yellow) filled with a relativistically-hot plasma, as characteristic of FRI jet sources.

have a qualitatively different morphology than the high-power jets. The movie shows the tips of low-power jets get periodically broken off by the kink instability. Such broken-off segments are potentially seen in 2-cm VLA images of the M87 jet at around 5 kpc (de-projected) away from the central BH (Owen, Hardee, & Cornwell 1989). The instability-induced erratic motion of the jet head slows down the jet propagation, spreads the jet exhaust over a large area, and inflates quasi-spherical cavities filled with a relativistically-hot magnetised plasma, as in FRI sources. This is very different from powerful jets that maintain their direction and speed and whose exhaust forms strong backflows, as in FRII sources (Fig. 4a,b).

The duration of the jet stall is dictated by the timescale for the cavity to double its radius and for its jet-confining pressure to drop substantially. After this, the jets regain their ability to propagate. However, they still remain strongly unstable to the kink mode and develop strong bends beyond the critical distance, $r_{\text{crit}} \sim 5$ kpc. Their dynamics from then on is a mixture of disruption and precession. Precession-induced periodic oscillations in the position of the jet head in model P44 are especially clearly seen in Fig. 3 at $t = 12\text{--}16$ Myr. To verify the robustness of the instability, we have repeated the low-power model P44 at twice as high effective resolution and refer to it as model P44HR (see Table 1). The positions of jet heads in both models agree very well (Fig. 3), indicating that our models are numerically-converged.

4 DISCUSSION AND CONCLUSIONS

We carried out novel simulations of relativistic AGN jets propagating in an ambient medium. The simulations, for the first time, are (i) global, (ii) 3D, (iii) magnetised, and (iv) launch jets self-consistently via the rotation of the central object. All 4 elements are crucial for capturing the global 3D magnetic kink instability that shapes relativistic jet feedback and interaction with the ISM/IGM. The kink instability grows on the timescale it takes Alfvén waves to travel around the jet ~ 10 times and becomes disruptive when its growth time is shorter than the fluid travel time from the base to the tip of the jet (Sec. 3). Thus, narrower jets are less stable.

A jet of power L_j propagating in a flat density profile $n = n_{\text{kpc}} \times (r/\text{kpc})^{-\alpha}$, with $\alpha \sim 1$ characteristic of galaxy/cluster cores, becomes progressively more collimated: $\gamma_j \theta_j \propto r^{(\alpha-2)/6}$ (eq. 1). Once θ_j drops below a critical value, $\theta_{\text{crit}} \equiv 0.03/\gamma_j$ (eq. 1), the instability becomes disruptive and stalls the jet. This occurs at a critical distance, $r_{\text{crit}} \propto (L_j/n_{\text{kpc}})^{1/(2-\alpha)}$ (eq. 2). The instability-induced erratic motions of the jet head slow down the jet, by spreading its exhaust over a larger area, and inflate quasi-spherical cavities, similar to what is observed in FRI sources (Fig. 4c). For high-power jets, r_{crit} is much larger than the flat density profile core radius, r_{core} . Such jets stably propagate in the flat density core region, break out of it, and remain stable to large distances. Their exhausts form powerful backflows, as observed in FRII sources (Fig. 4a,b). Thus, the magnetic kink instability can naturally lead to the Fanaroff & Riley (1974) dichotomy of AGN jets.

Inverting eq. (2) gives us a critical jet power,

$$L_{j,\text{crit}} = 4 \times 10^{44} \text{ erg s}^{-1} \frac{n_{\text{kpc}}}{0.2 \text{ cm}^{-3}} \left(\frac{r_{\text{core}}}{30 \text{ kpc}} \right)^{2-\alpha}, \quad (3)$$

above which a jet will stably escape out of the flat density profile core. This critical power, which sets the FRI/II dividing line, increases with the optical luminosity of a galaxy as $L_{j,\text{crit}} \propto L_{\text{opt}}^{1.8}$ (Ledlow & Owen 1996). To verify whether our model reproduces this scaling, we note that brighter galaxies have larger cores $r_{\text{core}} \propto L_{\text{opt}}^{1.1}$ (Faber et al. 1997) and lower core densities $n_{\text{core}} \propto L_{\text{opt}}^{-1/2}$ (PK15). Substituting these relations and the galaxy density profile $n_{\text{kpc}} \propto n_{\text{core}}(r_{\text{core}})^{-\alpha}$ into equation (3) gives $L_{j,\text{crit}} \propto n_{\text{core}} r_{\text{core}}^2 \propto L_{\text{opt}}^{1.7}$, in excellent agreement with the observed scaling.

PK15 performed *local* relativistic 3D MHD simulations of jets in periodic boxes and found that all laterally causally-connected jets eventually got disrupted by the magnetic kink instability. They argued that FRI jets are in lateral casual contact and FRII jets are not (see also Bicknell 1995). However, this would imply that all our jets beyond the recollimation point should be globally unstable, contrary to our findings. The difference is due to PK15 adopting periodic boundary conditions, which implied that their jets were infinitely long ($\gg r_{\text{crit}}$) and caused all their causally-connected jets to disrupt. KA97 constructed a 2D self-similar model of non-relativistic hydrodynamic jets. They postulated phenomenologically that once shear-induced instabilities penetrate from the shear layer to the axis of a jet, the jet morphology switches from FRII to FRI. They did not verify this claim with simulations. The physics underlying their model is vastly different than ours and so is their jet dynamics, however the two models share the same scaling of the jet opening angle and of the FRI/II transition with the jet length. That these predicted scalings are so insensitive to the underlying physical assumptions, highlights the need for first-principles, global relativistic 3D MHD simulations to constrain the basic jet physics.

Here, we set the confining medium at the Bondi radius and neglected other jet confining effects at smaller radii, e.g. by disk wind

(e.g., Hawley & Krolik 2006; McKinney 2006; Tchekhovskoy, McKinney, & Narayan 2008). This led to jets with order unity Lorentz factors. In the future, we plan to include disk wind effects which may lead to higher values of the Lorentz factor and affect the jet stability, morphology, and emission. We will also explore different density profiles, shapes of gravitational wells, and values of cluster rotation, to identify the physical processes in sources producing Mpc-scale FRI jets, e.g., 3C 31 (Hardcastle et al. 2002).

We neglected gravity, buoyancy effects, and the thermal pressure of the pristine ISM/IGM. The inclusion of the latter will only have a small effect on FRII jets, but it can increase the confining pressure of FRI jets and decrease their stability, strengthening our results. Over the simulated long time scale of ≥ 15 Myr the effects of buoyancy may eventually become important and can expel some of the jet-inflated cavities in the form of buoyant mushroom-like bubbles, such as those seen in the 90 cm radio image of the M87 galaxy ~ 20 kpc eastward of the core (Owen, Eilek, & Kassim 2000). Such slowly rising buoyant bubbles can heat up the intra-cluster medium (Zhuravleva et al. 2014, 2015; Soker 2016).

5 ACKNOWLEDGEMENTS

We thank S. Phinney, R. Laing, S. Markoff, A. Königl, D. Giannios, R. Barniol Duran, Ashley King, B. McNamara, M. Hardcastle, T. Piran, A. Spitkovsky and the anonymous referee for discussions and helpful comments. A.T. was supported by NASA through Einstein Postdoctoral Fellowship grant number PF3-140115 awarded by the Chandra X-ray Center, operated by the Smithsonian Astrophysical Observatory for NASA under contract NAS8-03060, and NSF through an XSEDE computational time allocation TG-AST100040 on TACC Stampede, Maverick, and Ranch, and NICS Darter. The simulations presented in this work also used the Savio cluster provided by UCB. A.T. thanks Skyhouse for hospitality. O.B. was supported by the Lyman Spitzer Jr. Fellowship, awarded by the Department of Astrophysical Sciences at Princeton University and the Max-Planck/Princeton Center for Plasma Physics.

REFERENCES

- Appl S., Lery T., Baty H., 2000, *A&A*, 355, 818
 Baum S. A., Zirbel E. L., O’Dea C. P., 1995, *ApJ*, 451, 88
 Best P. N., 2009, *Astronomische Nachrichten*, 330, 184
 Bicknell G. V., 1995, *ApJS*, 101, 29
 Biretta J. A., Sparks W. B., Macchetto F., 1999, *ApJ*, 520, 621
 Bromberg O., Tchekhovskoy A., 2016, *MNRAS*, 456, 1739
 Clarke D. A., Norman M. L., Burns J. O., 1986, *ApJ*, 311, L63
 Faber S. M. et al., 1997, *AJ*, 114, 1771
 Fanaroff B. L., Riley J. M., 1974, *MNRAS*, 167, 31P
 Gammie C. F., McKinney J. C., Tóth G., 2003, *ApJ*, 589, 444
 Ghisellini G., Tavecchio F., Maraschi L., Celotti A., Sbarro T., 2014, *Nature*, 515, 376
 Gopal-Krishna, Wiita P. J., 2000, *A&A*, 363, 507
 Guan X., Li H., Li S., 2014, *ApJ*, 781, 48
 Hagino K. et al., 2015, *ApJ*, 805, 101
 Hardcastle M. J., Worrall D. M., Birkinshaw M., Laing R. A., Bridle A. H., 2002, *MNRAS*, 334, 182
 Hawley J. F., Krolik J. H., 2006, *ApJ*, 641, 103
 Hines D. C., Eilek J. A., Owen F. N., 1989, *ApJ*, 347, 713
 Kaiser C. R., Alexander P., 1997, *MNRAS*, 286, 215
 Komissarov S. S., 1994, *MNRAS*, 269, 394
 Laing R. A., 1993, *Astrophysics and Space Science Library*, 103, 95
 Laing R. A., Bridle A. H., 2002, *MNRAS*, 336, 1161
 Laing R. A., Bridle A. H., Parma P., Feretti L., Giovannini G., Murgia M., Perley R. A., 2008, *MNRAS*, 386, 657
 Ledlow M. J., Owen F. N., 1996, *The Astronomical Journal*, 112, 9
 McKinney J. C., 2006, *MNRAS*, 368, 1561
 McKinney J. C., Blandford R. D., 2009, *MNRAS*, 394, L126
 Meier D. L., 1999, *ApJ*, 522, 753
 Meliani Z., Keppens R., 2009, *ApJ*, 705, 1594
 Meyer E. T., Sparks W. B., Biretta J. A., Anderson J., Sohn S. T., van der Marel R. P., Norman C., Nakamura M., 2013, *ApJ*, 774, L21
 Mignone A., Rossi P., Bodo G., Ferrari A., Massaglia S., 2010, *MNRAS*, 402, 7
 Million E. T., Werner N., Simionescu A., Allen S. W., Nulsen P. E. J., Fabian A. C., Böhringer H., Sanders J. S., 2010, *MNRAS*, 407, 2046
 Mizuno Y., Lyubarsky Y., Nishikawa K.-I., Hardee P. E., 2012, *ApJ*, 757, 16
 Nakamura M., Asada K., 2013, *ApJ*, 775, 118
 Nakamura M., Li H., Li S., 2007, *ApJ*, 656, 721
 Narayan R., Li J., Tchekhovskoy A., 2009, *ApJ*, 697, 1681
 Nemmen R. S., Tchekhovskoy A., 2015, *MNRAS*, 449, 316
 Noble S. C., Gammie C. F., McKinney J. C., Del Zanna L., 2006, *ApJ*, 641, 626
 Owen F. N., Eilek J. A., Kassim N. E., 2000, *ApJ*, 543, 611
 Owen F. N., Hardee P. E., Cornwell T. J., 1989, *ApJ*, 340, 698
 Owen F. N., Ledlow M. J., 1994, in *ASP Conf. Ser.*, Vol. 54, *The First Stromlo Symposium: The Physics of Active Galaxies*, Bicknell G. V., Dopita M. A., Quinn P. J., eds., *Astron. Soc. Pac.*, San Francisco, p. 319
 Perley R. A., Dreher J. W., Cowan J. J., 1984, *ApJ*, 285, L35
 Perucho M., Martí J. M., Cela J. M., Hanasz M., de La Cruz R., Rubio F., 2010, *A&A*, 519, A41
 Perucho M., Martí J. M., Hanasz M., 2005, *A&A*, 443, 863
 Perucho M., Martí J. M., Laing R. A., Hardee P. E., 2014, *MNRAS*, 441, 1488
 Porth O., Komissarov S. S., 2015, *MNRAS*, 452, 1089
 Russell H. R., Fabian A. C., McNamara B. R., Broderick A. E., 2015, *MNRAS*, 451, 588
 Soker N., 2016, *ArXiv:1605.02672*
 Stewart G. C., Fabian A. C., Nulsen P. E. J., Canizares C. R., 1984, *ApJ*, 278, 536
 Tchekhovskoy A., 2015, in *Astrophys. Space Sci. Libr.*, Vol. 414, *The Formation and Disruption of Black Hole Jets*, Contopoulos I., Gabuzda D., Kylafis N., eds., p. 45
 Tchekhovskoy A., McKinney J. C., 2012, *MNRAS*, 423, L55
 Tchekhovskoy A., McKinney J. C., Narayan R., 2007, *MNRAS*, 379, 469
 Tchekhovskoy A., McKinney J. C., Narayan R., 2008, *MNRAS*, 388, 551
 Tchekhovskoy A., McKinney J. C., Narayan R., 2012, *Journal of Physics Conference Series*, 372, 012040
 Tchekhovskoy A., Narayan R., McKinney J. C., 2011, *MNRAS*, 418, L79
 Wykes S., Hardcastle M. J., Karakas A. I., Vink J. S., 2015, *MNRAS*, 447, 1001
 Zamaninasab M., Clausen-Brown E., Savolainen T., Tchekhovskoy A., 2014, *Nature*, 510, 126
 Zhuravleva I. et al., 2015, *MNRAS*, 450, 4184
 Zhuravleva I. et al., 2014, *Nature*, 515, 85

SUPPORTING INFORMATION

Additional Supporting Information may be found in the online version of this article and on YouTube (link):

Movie files: movies of Fig. 4(a)-(c). (<http://www.mnras.oxfordjournals.org/lookup/suppl/doi:10.1093/mnras/slw064/-/DC1>).

Please note: Oxford University Press is not responsible for the content or functionality of any supporting materials supplied by the authors. Any queries (other than missing material) should be directed to the corresponding author for the Letter.